Rheologica Acta Rheol Acta 30:44–57 (1991)

A new constitutive model for fibre suspensions: flow past a sphere

N. Phan-Thien[1] and A.L. Graham[2]

[1]Department of Mechanical Engineering, University of Sydney, Sydney, Australia
[2]Mechanical and Electronic Engineering Division, Los Alamos National Laboratory, Los Alamos, New Mexico, USA

Abstract: A new phenomenological constitutive equation for homogeneous suspensions of macrosized fibres is proposed. In the model, the local averaged orientation of the fibres is represented by a director field, which evolves in time in a manner similar to the rotation of a prolate spheroid. The stress is linear in the strain rate, but the viscosity is a fourth-order tensor that is directly related to the director field. In the limit of low-volume fractions of fibres, the model reduces properly to the leading terms of the constitutive equation for dilute suspensions of spheroids. The model has three parameters: the aspect ratio R of the fibres, the volume fraction Φ, and A, which plays the role of the maximum-volume fraction of the fibres. Experimental shear data are used to estimate the parameter A, and the resulting model is used in a boundary-element program to study the flow past a sphere placed at the centre line of a cylinder for the whole range of volume fractions from 0.01 to near maximum volume fraction. The agreement with experimental data from Milliken et al. [1] is good.

Key words: Fibre suspensions; constitutive equation; flow past a sphere; boundary-element method

1. Introduction

The rheological behaviour of fibre suspensions has recently been a subject of interest owing to the increasing use of composite materials. Most of the rheological studies of fibre suspensions were concerned with determining the effective shear viscosity as a function of the volume fraction and the aspect ratio of the fibres. Past and recent progress was reviewed in Brenner [2], Metzner [3] and Ganani and Powell [4]. In nearly all of the experimental works, the fibres are large and rigid so that the effects of fluid inertia and Brownian motion are negligible. In general, it was found that the flow is intrinsically unsteady and the suspension is anisotropic in that the "effective viscosity" (obtained usually by a time average) depends to some extent on the flow system to which the fluid is subjected. In particular, the shear viscosity (obtained in a shear flow) is lower than the effective viscosity obtained from a falling sphere rheometry [1] at the same volume fraction. This anisotropy can be due to several reasons, including a flow-induced migration of the fibres, which renders the fluid inhomogeneous, and a local re-arrangement of the microstructure. There is also the effect of the initial orientation of the fibres: an initial random orientation of the fibres always yields the maximum effective viscosity (over an initial aligned orientation of the fibres) in the falling-sphere rheometry [5]. In this sense, the fluid has a large span of memory. However, within a particular flow system (shear-flow or falling-sphere rheometry), the fluid behaves essentially like a Newtonian fluid with regard to the functional dependence on the shear rate (linear). The falling-sphere data [1] further showed that the dilute regime, as manifested by the proportionality between the specific viscosity and the volume fraction, extends to a volume fraction of about 12.5% for a suspension of rods of aspect ratio of 19.8. For volume fractions between 12.5% and 23.15%, the specific viscosity increases with the cube of the volume fraction. Data from Milliken et al. [1] plus new evidence (unpublished data [6]) on the flow-induced migration in suspensions using the Nuclear Magnetic Resonance (NMR) technique support the falling-sphere rheometry as the only practical method of measuring the suspension viscosity without unduly disturbing the microstructure.

Theoretical progress in fibre suspensions has been slow. Early works [7, 8] assumed that the stress field remains unaltered by the presence of the fibres and calculated the fibre trajectory by following its Jeffery's orbit [9]. As pointed out by Lipscomb et al. [10], such a calculation may be grossly in error, because the streamlines can be drastically altered even at fibre concentrations of less than 0.1%. An example is the 4:1 entry-flow problem, where the kinematics can change significantly from the Newtonian kinematics [10]. This change is brought about by the presence of the elongational flow along the centreline of the tube and the fact that a dilute suspension of fibres can sustain substantially larger tensile stresses than those in shear flow at a comparable deformational rate [11 – 13]. The finite element calculations of the 4:1 contraction-flow problem (Lipscomb et al. [10]), using a constitutive equation for a dilute suspension of prolate spheroids and the full-alignment assumption, showed excellent agreement with the experimental data on suspensions of chopped-glass fibres of aspect ratio 276 and at volume fraction less than 0.11%. The constitutive equation used in [10] is of the form of the Transversely Isotropic Fluid (TIF) model of Ericksen [14]. The connection of the TIF model with a dilute suspension of ellipsoids has been elucidated by several authors (Giesekus [15], Hand [16], Cox and Brenner [17], Leal and Hinch [18, 19]). It is noted that there are only two parameters appearing in the model: the volume fraction Φ and the aspect ratio of the ellipsoids R. The same constitutive equation was used in a finite-element [20] and a boundary-element simulation of the flow past a sphere (Phan-Thien et al. [21]).

It was found that the flow kinematics are intrinsically unsteady [21], and that the prediction of the effective viscosity (which is proportional to the time-averaged drag force on the sphere) agrees reasonably well with Milliken et al.'s data [1] at volume fractions less than 10%. At higher volume fractions, the effective specific viscosity was observed to increase with the cube of the volume fraction. The constitutive model, being a model for a dilute suspension, can only predict that the specific viscosity is proportional to the volume fraction; the transition from linear to cubic behaviour in the specific viscosity vs the volume fraction is outside the scope of the dilute-suspension theory.

The dilute constitutive theory, however, has several attractive features that have been observed experimentally with suspensions of rods. It is anisotropic, it is intrinsically unsteady in flows that have a shear component (e.g., shear flow, 4:1 contraction flow, flow past a sphere) and it has only two parameters (Φ and R), which have precise physical meaning. It is the intention of this study to extend this theory to the semi-dilute regime so that the transition from linear to cubic behaviour referred to earlier can be predicted. The modification is based on the observation that the rotation of a spheroid in a three-dimensional cubic array subjected to a bulk shearing flow [22] is only weakly dependent on the volume fraction, for $0 < \Phi < 0.13$. Thus, one can assume that the rotation of the spheroids is still given the Jeffery's solution up to a moderate volume fraction, at least, and modify the functional dependence of the parameters that appear in the TIF model so that the desired transition can be effected. We only insist that the modified constitutive equation goes to the correct limit at low-volume fractions. The new constitutive model has one additional parameter, A, which plays the role of the maximum-volume fraction. The shear flow data by Kitano et al. [23] on various fibre suspensions suggested that A decreases linearly with the aspect ratio R for a limited range of aspect ratios from 5 to 30; at the aspect ratio of 20, $A \approx 0.27$. The form of the constitutive equation is precisely that proposed by Evans [24] and Dinh and Armstrong [25] using a mean-field of random orientation.

The new constitutive equation was implemented in a boundary-element program, and the flow past a sphere placed at the centreline of a tube is studied next. Much of the interest in this flow has been generated from the possibility of measuring the effective viscosity by observing the fall of precision spheres through the fluid of interest. The apparatus required is relatively simple to construct and the underlying theory for Newtonian fluids is well understood. When the fluid is non-Newtonian, the problem is considerably more complex and the final analysis depends on the particular fluid model adopted. The flow problem is incidentally a benchmark problem set in the Fifth Workshop on Numerical Methods in Non-Newtonian Flows [26 – 28].

Most of the theoretical studies of the non-Newtonian flow past a sphere were based on perturbation and variational methods; a review of this is found in Acharya et al. [29]. Such results are limited to slightly non-Newtonian fluids or to inelastic generalized Newtonian fluids [30]. Numerical studies using finite difference [31, 32], finite element [33 – 36] and boundary element methods [21, 28, 37] have also been attempted. Most recent numerical works concentrated on the uniform flow of the Oldroyd-B fluid past a sphere placed at the centreline of a cylindrical tube [27, 28]. The quantity of interest to experimenters is

the drag coefficient χ defined by

$$\chi = \frac{F}{F_N} ,$$

where F is the drag force on the sphere and F_N is the corresponding drag force for a Newtonian fluid of the same viscosity.

The new constitutive equation is similar in form to the TIF model, and thus we find no steady-state solution to the flow past a sphere [21]. The effective reduced viscosity (η_r) obtained by time-averaging the drag force on the spheres and normalizing the result with respect to the Newtonian drag force agrees reasonably well with Milliken et al.'s data [1], using $A = 0.27$ as suggested by Kitano et al.'s data [23]. However, the plot of the specific viscosity ($\eta_{sp} = \eta_r - 1$) vs the volume fraction reveals that the nonlinear transition occurs at a volume fraction of about 7.5%. For this transition to occur at 12.5%, as observed by Milliken et al. [1], A has to be about 0.46. At high-volume fractions, a scaled problem is solved to supply an asymptotic formula for the reduced viscosity. It is found that the reduced viscosity predicted by the falling-sphere method can be considerably greater than the reduced shear viscosity; at the aspect ratio of $R = 20$, it can be seven times higher. The initial orientation of the fibres has a negligible effect on the averaged drag force on the sphere over a long time. Over a short time ($t < 10$), however, the averaged drag force is highest when the initial orientation of the fibres is randomized.

2. Constitutive equation

2.1 The model

The simplest properly invariant theory of anisotropic fluids is the Transversely Isotropic Fluid (TIF) model proposed by Ericksen [14]. In this model the microstructure of the fluid is characterised by a unit vector field $\boldsymbol{p}$, which evolves in time according to a certain law. The stress generated by the microstructure is a tensor-value function of this unit vector field and the strain rate tensor.

Jeffery [9] considered the motion of a rigid spheroid suspended in a Newtonian fluid. He showed that the spheroid translates with the fluid velocity and rotates according to

$$\frac{D\boldsymbol{p}}{Dt} = \boldsymbol{W}\cdot\boldsymbol{p} + \frac{R^2-1}{R^2+1}(\boldsymbol{D}\cdot\boldsymbol{p} - \boldsymbol{D}:ppp) , \qquad (1)$$

where $D(\cdot)/Dt$ is the material derivative, $\boldsymbol{W} = ((\nabla\boldsymbol{u})^\dagger - \nabla\boldsymbol{u})/2$ is the vorticity tensor, $\boldsymbol{D} = ((\nabla\boldsymbol{u})^\dagger + \nabla\boldsymbol{u})/2$ is the strain-rate tensor, the † denotes the transpose operation, R is the aspect ratio of the spheroid as before and $\boldsymbol{p}$ is a unit vector along the major axis of the spheroid. Note that as $\dot{\boldsymbol{p}}\cdot\boldsymbol{p} = 0$, the magnitude of $\boldsymbol{p}$ is preserved in this time evolution. If $\boldsymbol{p}$ is initially a unit vector, then it remains a unit vector at all time.

Giesekus [15], Hand [16], Cox and Brenner [17], Leal and Hinch [18, 19], Evans [24], amongst others, considered a dilute suspension of monosized rigid spheroids and obtained the volume-averaged stress using Jeffery's solution. They showed that the TIF model is appropriate continuum description of the suspension. In this case, the unit vector field $\boldsymbol{p}$ is simply the unit vector along the axis of the spheroid and the bulk stress generated by the microstructure is given by [18]

$$\boldsymbol{S} = 2\eta\boldsymbol{D} + 2\eta\Phi\{A'\boldsymbol{D}:pppp + B(\boldsymbol{D}\cdot pp + pp\cdot\boldsymbol{D}) + C\boldsymbol{D} + d_R F pp\} , \qquad (2)$$

where η is the viscosity of the solvent, Φ is the volume fraction, d_R is the rotational diffusivity of the spheroids and A', B, C, F are material constants depending on the aspect ratio of the microstructure. The asymptotic values of A', B, C and F are tabulated in Table 1.

Equation (2) should be further averaged with respect to the probability distribution of $\boldsymbol{p}$. However, we are concerned with a dilute suspension of macrosized fibres (large aspect ratio) so that the diffusivity can be set to zero, and we feel free to write $\langle\boldsymbol{p}\rangle$ interchangeably with $\boldsymbol{p}$, where the angular brackets denote the ensemble average. Physically, $\boldsymbol{p}$ can be regarded as either the local orientation of an individual fibre or the mean orientation of the fibres locally. The size of the fibres must, however, be considerably smaller than any relevant length scale of the problem for the suspension to be treated as a continuum. It is interesting to note that Milliken et al. [1] found that falling spheres smaller than the length of the fibres give the same average viscosity as much larger spheres; that is, the continuum hypothesis holds at a length scale comparable to the length scale of the fibres. Furthermore, the implication of the dilute assumption for a suspension of fibres is that $\Phi R^2 \ll 1$. However, Milliken et al.'s data [1] showed that the dilute regime extends to $\Phi R^2 \approx 50$.

Table 1. Asymptotic values of A', B, C and F

Asymptotic limits	A'	B	C	F
$R\to\infty$ (rodlike)	$\frac{R^2}{2(\ln 2R-1.5)}$	$\frac{6\ln 2R-11}{R^2}$	2	$\frac{3R^2}{\ln 2R-0.5}$
$R=1+\delta$, $\delta\ll 1$ (near sphere)	$\frac{395}{147}\delta^2$	$\frac{15}{14}\delta-\frac{395}{588}\delta^2$	$\frac{5}{2}\left(1-\frac{2}{7}\delta+\frac{1}{3}\delta^3\right)$	9δ
$R\to 0$ (disklike)	$\frac{10}{3\pi R}+\frac{208}{9\pi^2}-2$	$-\frac{8}{3\pi R}+1-\frac{128}{9\pi^2}$	$\frac{8}{3\pi R}$	$-\frac{12}{\pi R}$

Note that, from Eq. (1)

$$\frac{Dpp}{Dt} = W\cdot pp - pp\cdot W + \frac{R^2-1}{R^2+1}(D\cdot pp + pp\cdot D - 2D:pppp) \ .$$

This is identical to the constitutive equation adopted by Lipscomb et al. [10] for solving the 4:1 entry-flow problem. As a consequence of their closure assumption $D:\langle pppp\rangle = D:\langle pp\rangle\{pp\rangle$ (their Eq. (24)), their $\langle pp\rangle$ is equivalent to pp in our notation and, thus, the constitutive equation adopted in [10] and also in [20], although written in terms of $\langle pp\rangle$, is mathematically the same as the constitutive equation adopted in the boundary element study [21]. Note, however, that in the finite-element studies [10, 20], the fully alignment assumption was adopted. This assumption replaces p by $u/|u|$, which is the equilibrium solution near a solid surface for fibres with infinite-aspect ratio.

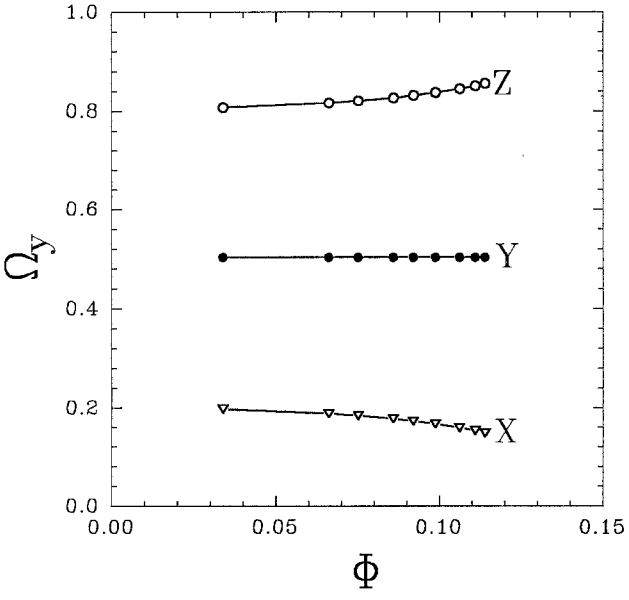

Fig. 1. Angular velocity Ω_y of a prolate spheroid in a cubic array arrangement under a bulk shearing flow in the $x-z$ plane. The bulk shear rate is 1. The aspect ratio of the spheroid is 2. The curves labelled X, Y and Z are the results for spheroids aligned in the x, y and z direction, respectively. Jeffery's solution [9] shows that these angular velocities should be 0.2, 0.5 and 0.8, respectively, for the three cases mentioned above

The TIF model, represented by Eqs. (1) and (2), is quite successful in describing certain qualitative features of suspensions. It predicts that both the shear stress and the first normal-stress difference are linear in the shear rate $\dot\gamma$ in a simple shearing flow. In addition, the stresses are functions of $\dot\gamma t$, where t is the time. These features have been observed in experiments [38] with suspensions of polystyrene spheres (diameters in the range $40-50\,\mu$m) in a silicon oil. However, the stresses are periodic in time, which corresponds directly with the Jeffrey orbits executed by spheroids [9] and has been observed in dilute suspensions [39].

In a recent numerical simulation of a simple shearing flow past a cubic array of prolate spheroids (of aspect ratio 2), we find that the rotation of the spheroids is only weakly dependent on the volume fraction, up to a volume fraction of 0.11 (the maximum volume fraction of a cubic array of prolate spheroids of aspect ratio 2 is $\pi/24\approx 0.13$). Figure 1 shows this clearly. In this figure, the curves labelled X, Y and Z represent the angular velocity of the spheroids aligned in the x, y and z direction, respectively. The bulk shearing flow takes place in the $x-z$ plane. Equation (1) predicts that the angular velocities in these three cases are 0.2, 0.5 and 0.8, respectively. Thus, it seems reasonable to assume that the spheroids rotate according to Eq. (1) up to moderate volume fractions.

To make the connection between the director field p and the stress tensor, we note that the dominant term in Eq. (2) at large aspect ratios is the term involving A'. However, this term is proportional to the volume fraction and no non-linear transition is possible. We, therefore, assume that the stress is given by

$$S = 2\eta D + 2\eta f(\Phi, R) D : pppp \ , \tag{3}$$

where f is a function, yet to be determined, of the volume fraction and the aspect ratio. In the limit of vanishing volume fraction, this constitutive equation should reduce to the dominant terms of Eq. (2). Thus, we require that

$$\lim_{\Phi \to 0} f(\Phi, R) = \frac{R^2 \Phi}{2(\ln 2R - 1.5)} \ .$$

Our new phenomenological equation, as represented by Eqs. (1) – (3), is motivated by the constitutive equation of dilute suspensions of fibres; its usefulness should be judged by its ability to fit experimental data. Note that the form of the constitutive equation is precisely that proposed by Evans [24] and Dinh and Armstrong [25]; the functional dependence of f on the volume fraction Φ, however, is determined by a mean-field assumption of random orientation [40].

2.2 *Simple shear flow*

To determine the functional form for the function $f(\Phi, R)$, we consider the simple shearing flow with shear rate $\dot{\gamma}$. In this flow, p is periodic in time:

$$p_1 = (\alpha \cos \omega t + \beta \sin \omega t)/P \ ,$$

$$p_2 = \sqrt{\frac{\zeta}{2-\zeta}} (\beta \cos \omega t - \alpha \sin \omega t)/P \ ,$$

and

$$P = \sqrt{(\alpha \cos \omega t + \beta \sin \omega t)^2 + \frac{\zeta}{2-\zeta} (\beta \cos \omega t - \alpha \sin \omega t)^2} \ ,$$

where α and β are constants related to the initial values of p, and the frequency ω is given by

$$\omega = \frac{1}{2} \sqrt{\zeta(2-\zeta)\dot{\gamma}^2} \ , \quad \zeta = \frac{2}{R^2 + 1} \ ,$$

which is proportional to the magnitude of the shear rate.

The instantaneous viscosity is defined by the ratio of the shear stress to the shear rate; it is given by

$$\eta_{\text{ins}} = \eta [1 + 2 f(\Phi, R) p_1^2(t) p_2^2(t))] \ .$$

Because p is a periodic function of time, the instantaneous viscosity is also a periodic function of time. We take the experimental approach of using the time-average value to define the effective viscosity:

$$\eta_{\text{eff}} = \eta [1 + 2 f(\Phi, R) \langle p_1^2(t) p_2^2(t) \rangle] \ ,$$

where the angular brackets now denote the time average. From the solutions for $p_1(t)$ and $p_2(t)$, it is found that $\langle p_1^2 p_2^2 \rangle$ is proportional to $1/R^2$. Thus, the reduced viscosity is

$$\eta_r = \frac{\eta_{\text{eff}}}{\eta} = 1 + c \frac{f(\Phi, R)}{R^2} \ , \tag{4}$$

where c is a constant.

To obtain a specific functional form for f, we recourse to an empirical relation proposed by Kitano et al. [23]. These authors obtained shear viscosities of various suspensions of inorganic fillers (glass fibres, carbon fibres, talc, precipitated- and natural-calcium carbonate powder) of aspect ratios in the range 6 – 28. They found that the empirical equation

$$\eta_r = \frac{1}{(1 - \Phi/A)^2} \ , \tag{5}$$

can be used to correlate their data, provided that the parameter A is fitted to the properties of the particular suspension at hand; A is basically the maximum volume fraction of the suspension. A linear regression through their data (Fig. 2) shows that A can be approximated by the linear relation

$$A = 0.53 - 0.013 R \ , \quad 5 < R < 30 \ . \tag{6}$$

If we require that the predicted reduced viscosity has the same functional form as observed by Kitano et al. [23] at $\Phi/A \to 1$, and yet has the correct form in the limit of low-volume fraction, then a simple functional form for f is

$$f(\Phi, R) = \frac{R^2 \Phi (2 - \Phi/A)}{4(\ln 2R - 1.5)(1 - \Phi/A)^2} \ . \tag{7}$$

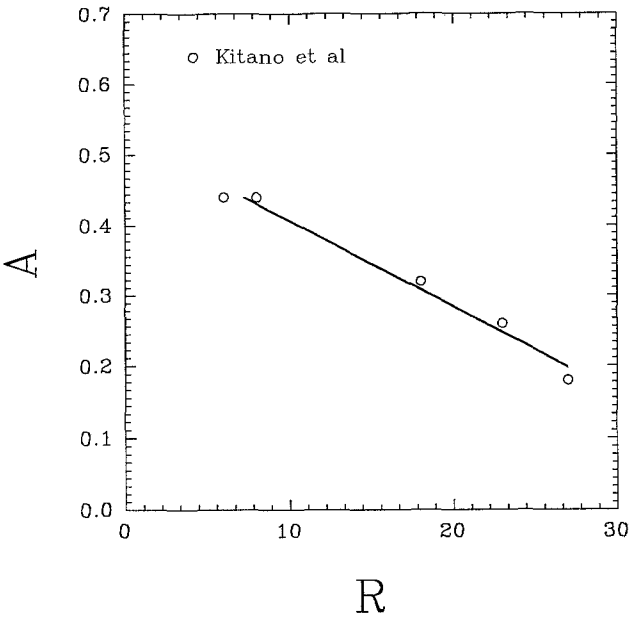

Fig. 2. Dependence of the maximum volume fraction A on the fibre aspect ratio. Data from Kitano et al. [22]

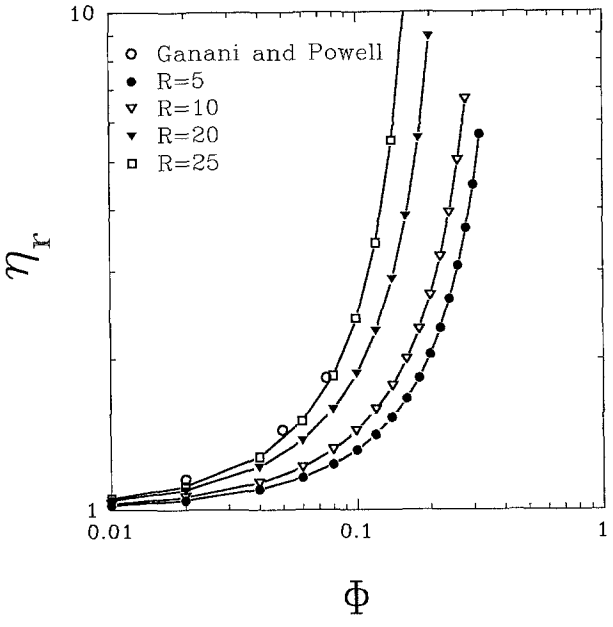

Fig. 3. Reduced viscosity in a simple shearing flow. Data (○) from Ganani and Powell [37]

In summary, the proposed constitutive equation has a director field that evolves in time according to Jeffery's solution [Eq. (1)], a stress rule [Eq. (3)] that allows the calculation of the stresses given $\boldsymbol{p}$ and the velocity gradient. The stress rule involves three parameters: the volume fraction Φ, the aspect ratio R, and the maximum volume fraction A. The evolution equation of the director field only involves the aspect ratio; it is not obvious how to build in the Φ-dependence into this equation at this stage. The maximum volume fraction is assumed to be given by Eq. (6) if the aspect ratio is between 5 and 30. There are no further adjustable parameters in the model, except the initial orientation of the fibres. Note that the volume fraction only enters the governing equations through the stress rules. The time evolution of the fibres' orientation is affected by the volume fraction indirectly via the kinematics.

In the simple shearing flow, the time-averaged value of $p_1^2 p_2^2$ depends only weakly on the initial orientation of the fibres for $5 < R < 30$. The reduced shear viscosity can be shown to take the form

$$\eta_r = 1 + k \frac{\Phi(2 - \Phi/A)}{(1 - \Phi/A)^2} , \tag{8}$$

where k is evaluated from the average of $p_1^2 p_2^2$ and the aspect ratio of the fibres. It is found that $k = 1.09$, 1.40, 2.10 and 2.46 for $R = 5$, 10, 20 and 25, respectively. The intrinsic viscosity of the suspension is

$$[\mu] = \lim_{\Phi \to 0} \frac{\eta_r - 1}{\Phi} = 2k .$$

At the aspect ratio of 20, the intrinsic viscosity as measured in a simple shear flow is predicted to be about 4.2, which is considerably smaller than the value 28.5 as measured in falling-sphere rheometry [1].

The reduced shear viscosity is plotted in Fig. 3 for the four different aspect ratios. The shear-flow data from Ganani and Powell [41] for $R = 25$ are also included in Fig. 3. The agreement between the prediction and the experimental data is reasonable. In Fig. 4, the specific viscosity $\eta_{sp} = \eta_r - 1$ is plotted against the volume fraction. For the aspect ratio of 20, the non-linear behaviour in the plot of η_{sp} vs Φ sets in at a volume fraction of about 0.10. For $\Phi < 0.10$, η_{sp} is proportional to the volume fraction, and with a limited number of data points between $0.1 < \Phi < 0.2$, one can certainly fit a cubic relation to the $\eta_{sp} - \Phi$ curve. This "transition" from linear to cubic behaviour for this model suspension is, of course, an artifact of the method of plotting, and has nothing to do with transition at microstructural level.

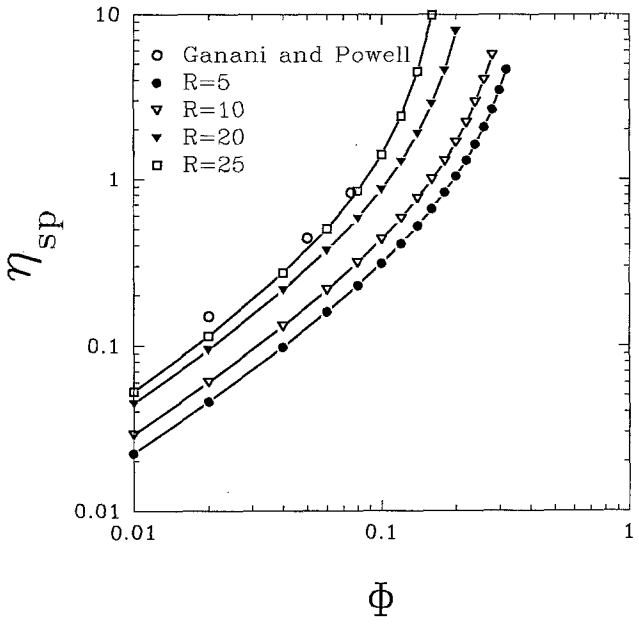

Fig. 4. Specific viscosity in a simple shearing flow. Data (○) from Ganani and Powell [37]

The instantaneous normal stress differences are given by

$$N_1 = 2\eta\dot{\gamma}f(\Phi,R)p_1(t)p_2(t)(p_1^2(t)-p_2^2(t)) \ ,$$

$$N_2 = -N_1 \ , \tag{9}$$

where $\dot{\gamma}$ is the shear rate. The time-average of the normal stress differences, however, is zero at all aspect ratios. It should be noted that this constitutive equation is linear in the strain-rate tensor; all properties (such as drag force and stresses) should be linear in the strain rate. The strain rate can, therefore, be factored out of the numerical problem.

The fact that the kinetics are periodic in time in the simple shearing flow suggests that there is no guarantee of having a steady-state solution in complex flows, at least in those that have a shear flow component in parts of the flow domain. The numerical method adopted to solve the TIF or the new model must necessarily be a time-dependent method; furthermore, the time integration scheme must be robust enough to handle fast-varying stresses.

2.3 Elongational flow

In a uniaxial elongational flow, in which the strain-rate tensor takes the form

$$\boldsymbol{D} = \text{diag}\,(2G, -G, -G) \ ,$$

where $G>0$ is the strain rate, it can be easily shown that

$$\lim_{t\to\infty} \boldsymbol{p}(t) = \{1,0,0\} \ .$$

The Trouton, or elongational viscosity is given by

$$\eta_T = 3\eta + 2\eta f(\Phi,R) \ . \tag{10}$$

The reduced Trouton viscosity is given precisely by Eq. (8), where

$$k = \frac{R^2}{3\,(\ln 2R^2 - 1.5)} \ .$$

At $R = 25$, $k = 86.4$, which is about 35 times greater than the corresponding value in shear flow.

3. Flow past a sphere

3.1 Problem formation

We consider next the flow generated by a sphere falling along the centreline of a cylindrical tube containing the model suspension fluid. The radius of the sphere is a, and the radius of the tube is $2a$ (these are the dimensions recommended by the Fifth Workshop in Numerical Methods in Non-Newtonian Flows). In a frame of reference that translates with the sphere, the sphere is at rest and the tube wall is seen moving with a constant velocity (the falling speed U of the sphere, but in the opposite direction of the falling sphere). Henceforth, all length scales are normalized with respect to a and velocities are normalized with respect to U; the time is therefore made dimensionless with respect to a/U. Furthermore, the fluid far away from the sphere is seen moving rigidly with the tube, and all associated stresses are zero there. The two equations we wish to solve are,

$$\nabla\cdot\boldsymbol{u} = 0 \quad \text{and} \quad \nabla\cdot\boldsymbol{\sigma} = 0 \ ,$$

subjected to the above-mentioned boundary conditions, in which $\boldsymbol{u}$ is the velocity field and $\boldsymbol{\sigma}$ is the total stress field given by

$$\boldsymbol{\sigma} = -P\mathbf{1} + \boldsymbol{S} \ ,$$

where P is the hydrodynamic pressure, $\mathbf{1}$ is the unit tensor and $\boldsymbol{S}$ is the "extra" stress given by Eq. (3).

The numerical method adopted is the boundary-element method (BEM), which has been described in several papers [37, 42] and needs not be repeated here

in detail. In essence, the method solves a series of linear problems, each with a known body force (the domain integrals of the extra non-Newtonian stresses), until convergence is achieved. The difference between the previous BEM [37] and the present scheme is the constitutive equation chosen and the method for computing the extra stresses. Sugeng and Tanner [37] employed a streamline scheme, whereas a time-integration scheme similar to that used in [42] is employed here.

A streamline scheme can be developed here by first defining a vector $\boldsymbol{q}$, which evolves in time according to

$$\dot{\boldsymbol{q}} = \mathscr{L} \cdot \boldsymbol{q} \ , \tag{11}$$

where $\mathscr{L}$ is an 'effective' velocity gradient yet to be determined and the super dot denotes the material time derivative. Let $\boldsymbol{p}$ be the unit vector along $\boldsymbol{q}$, i.e.,

$$\boldsymbol{p} = \frac{\boldsymbol{q}}{q} \ . \tag{12}$$

Thence

$$\dot{q} = \dot{\boldsymbol{q}} \cdot \boldsymbol{p} = q \mathscr{L} : \boldsymbol{pp} \ ,$$

and thus $\boldsymbol{p}$ evolves in time according to

$$\dot{\boldsymbol{p}} = \mathscr{L} \cdot \boldsymbol{p} - \mathscr{L} : \boldsymbol{ppp} \ .$$

This is identical to (1) if the 'effective' velocity gradient tensor is given by $\mathscr{L} = \boldsymbol{L} - \zeta \boldsymbol{D}$, where $\zeta = 2/(R^2+1)$. At infinite aspect ratio and in a homogeneous flow, Eq. (11) is the equation defining the velocity, and thus the solution for $\boldsymbol{p}$ is simply $\boldsymbol{u}/|\boldsymbol{u}|$. This is essentially the basis of the full alignment assumption. In an inhomogeneous flow and/or a finite-aspect ratio, the full alignment assumption will no longer provide a good solution to $\boldsymbol{p}$. We will not, therefore, adopt the full-alignment assumption here.

Along a streamline, the material derivative is simply the arc-length derivative. Thus, given the boundary conditions at the entry of the flow domain and the kinematics, Eq. (11) can be integrated along the streamline. The unit-vector field $\boldsymbol{p}$ can be found from Eq. (12), and hence the stress tensor can be found from Eq. (2). This scheme was implemented in the current BEM. However, we found that it is not very robust, especially with a fine mesh when the kinematics have yet to converge. In this case, streamline crossing may occur, leading to a divergence of the numerical results.

The time integration scheme (fourth-order Runge Kutta), which is based on integrating Eq. (11) using available current information, is much more robust, and was adopted in this study. Another advantage of the time-integration method is its ability to cope with recirculatory regions; actually there are none in this problem.

We first test the numerical method for the unbounded flow of the Newtonian fluid past a sphere. In this case, the drag force on the sphere is simply $6\pi\eta Ua$, where η is the fluid viscosity and U is the speed of the sphere. The rate of convergence is quadratic in the number of elements; with 360 elements, we obtained the drag force on the sphere correct to five significant figures [21]. We have also carried out similar numerical experiments for the flow past oblate and prolate spheroids. In both cases, the aspect ratio of the spheroids was varied from 2 to 1000. In all cases, we obtain five significant figures in accuracy when the number of boundary elements is about 300.

Next, we test the robustness of the time integration scheme in the simple shearing flow. Good agreement between the boundary element results and the exact results is obtained, even with a large time step of 0.05.

We consider now the flow past a sphere placed at the centreline of a tube. Different meshes with varying degrees of coarseness used in the study are listed in Table 2 and shown in Fig. 5a – c; only the results from the finest mesh are reported here (mesh M3). The half length of the cylinder is chosen to be $6a$ and the ratio of sphere-to-cylinder radius is 0.5.

The boundary conditions are:

- At the entry of the flow domain ($z = -6a$) plug flow conditions are applied, where the axial velocity $u = U$, the radial velocity $v = 0$.
- Along the tube wall ($r = a$) $u = U$ and $v = 0$.
- Along the centreline ($r = 0$) symmetry boundary conditions apply, where $v = 0$ and the axial traction $t_x = \sigma_{rz} = 0$.
- On the surface of the sphere $u = 0 = v$.
- At the outlet of the flow domain ($z = 6a$), the axial traction is set to zero (no net force action on the fluid) and the radial velocity $v = 0$.

Table 2. Summary of the boundary element meshes used for the calculations

Name	Boundary elements	Domain cells	Smallest BE length
M1	52	240	$0.262a$
M2	96	640	$0.157a$
M3	132	1456	$0.105a$

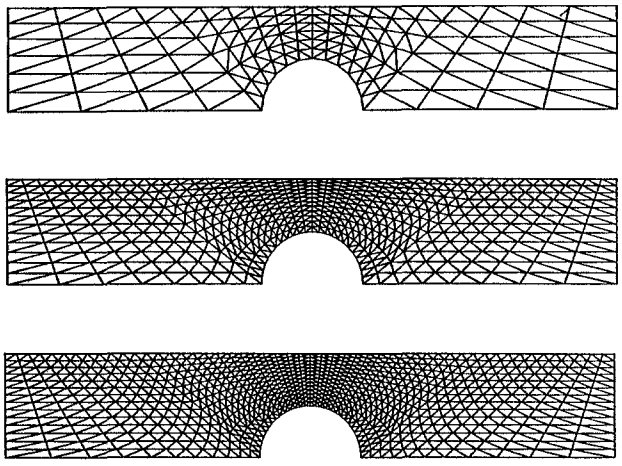

Fig. 5. Meshes for boundary-element calculations. Results reported in this paper are obtained with mesh M3: a) M1, b) M2, c) M3

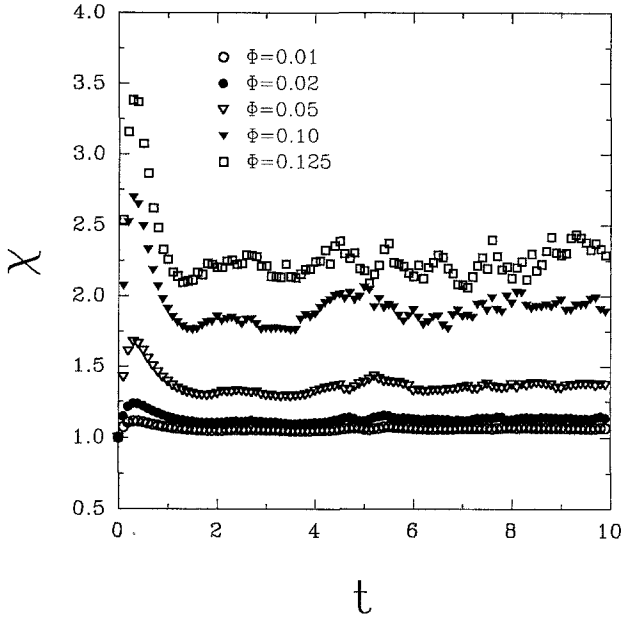

Fig. 6. Dimensionless drag force (normalized with respect to the Newtonian drag force, which is also obtained by the boundary-element method in the first iteration) as a function of time at different volume fractions. $R = 10$, $\theta = 90$ (fibres are initially perpendicular to the tube axis)

In addition, all stress components are set to zero and $\boldsymbol{p}$ is set to a known vector initially. We usually consider three cases:

1) Director $\boldsymbol{p}$ is initially aligned with the tube axis, or $\theta = 0$, where θ is the angle between $\boldsymbol{p}$ and the tube axis.
2) Director $\boldsymbol{p}$ is initially perpendicular to the tube axis, or $\theta = 90°$.
3) Director $\boldsymbol{p}$ is initially randomized; θ is chosen from a sequence of pseudo-random numbers between $-180°$ and $180°$.

3.2 Reduced viscosity

When the wall effects are considered, the Stokes drag for the Newtonian fluid can be estimated from the value of the unbounded case, using the Bohlin formula (see, for example, [43]):

$$\chi = [1 - 2.10444(a/R) + 2.08877(a/R)^3 - 0.94813(a/R)^5 - 1.372(a/R)^6 + 3.87(a/R)^8 - 4.19(a/R)^{10}]^{-1} , \quad (13)$$

where χ is the dimensionless drag force (with respect to Stokes drag $6\pi\eta Ua$). For the geometry under consideration, Eq. (13) predicts $\chi = 5.923$. The theory of Haberman [43] predicts the value to be 5.970. Recent careful finite-element [27] and boundary-element [28] studies showed this value to be 5.943. Our numerical results give $\chi = 5.777$, 5.900 and 5.919 from mesh M1, M2 and M3, respectively, for the Newtonian case.

For the TIF model, we found that the flow is intrinsically unsteady [21]. This model is a slight variation of TIF, and it is not surprising that we find the flow intrinsically unsteady. A plot of the dimensionless drag force χ (with respect to the Newtonian value in the same geometry) vs time is given in Fig. 6 for the aspect ratio $R = 10$ and $\theta = 90°$. The drag force appears random in time, especially at high volume fraction. The reason for the random nature of the drag force vs time was explained in [2]: in a simple shear flow, $\boldsymbol{p}$ is a periodic function with a frequency proportional to the magnitude of the shear rate, and so is the shear stress. In this problem, one has a spectrum of shear rates from 0 to a maximum shear rate on the sphere's surface. The local traction on the sphere's surface is also a periodic function of time, with a frequency that depends on the local shear rate. The drag force on the sphere is the area integral of the traction, and it should contain a spectrum of frequencies. It is the broad-band frequency spectrum that makes the plot of the drag force against time appear random. Note that there is an initial overshoot in the drag force vs time, presumably due to the re-arrangement of the fibres, followed by a fluctuation about a mean value. The fluctuation increases with the volume fraction; at $\Phi = 0.10$ and $R = 10$, the fluctuation is about 7% of the mean value. This increases to about 11% at $\Phi = 0.125$.

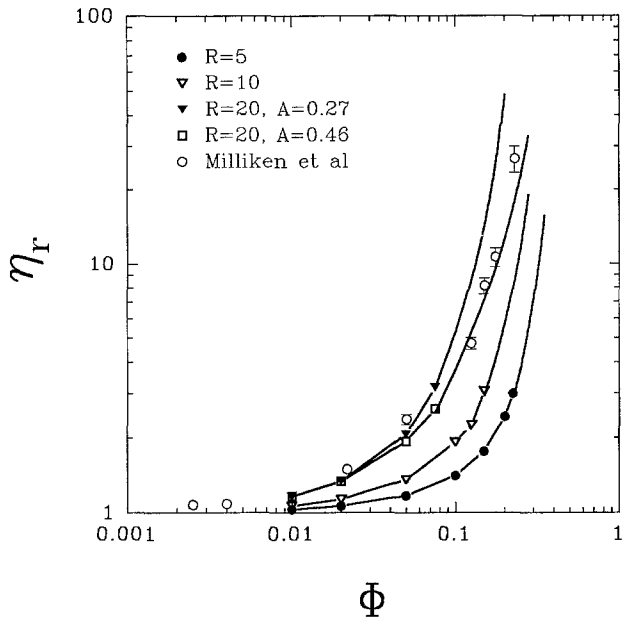

Fig. 7. Reduced viscosity, obtained by taking time averages of the dimensionless-drag force, as a function of the volume fraction. Errors on the reduced viscosity can be estimated using the standard deviation of the time averages taken at different time intervals. In all cases $\theta = 90$. Data (○) from Milliken et al. [1] for well-stirred (randomized) suspensions blunt-ended rods and fibres of aspect ratio 19.8. Solid lines connecting the last numerical data point are not the lines of best fit through the data; they are the asymptotic results discussed in Sect. 3.3

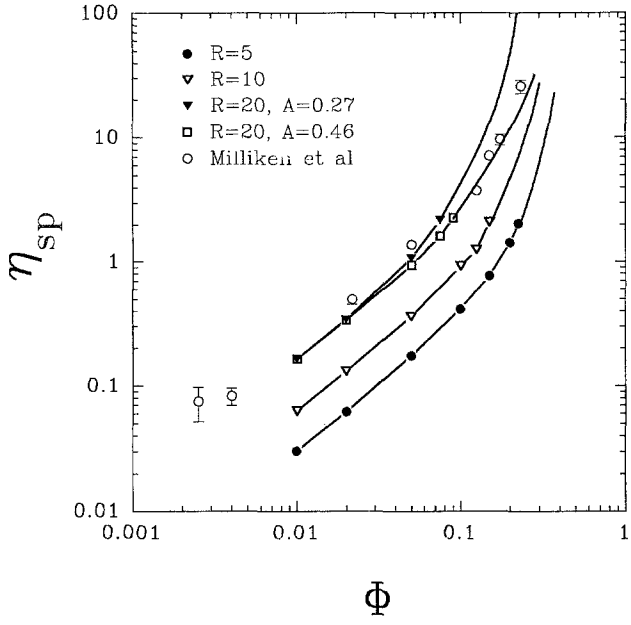

Fig. 8. Same as in Fig. 7, but for the specific viscosity. Transition from linear to cubic regime, as observed by Milliken et al. [1], can be mimiced by the theory using $A = 0.46$. Note that the transition suggested by the numerical results is an artifact of the method of plotting, and the limited range of volume fractions is considered. Had the asymptotic line extended beyond a volume fraction of 0.25, then the cubic behaviour was no longer present

The dimensionless drag force with respect to the Newtonian value in the same flow geometry is, in fact, the flow resistance felt by the sphere, or simply the reduced instantaneous viscosity. To calculate the reduced viscosity, we simply take the time-averaged value of the dimensionless drag, from $t = 4$ to $t = 10$ for suspensions of fibres of aspect ratio less than 10. At higher aspect ratios, it is necessary to take the average over a long time interval due to the large period of the oscillation in $\boldsymbol{p}$. In the simple shear flow, the period of oscillation in $\boldsymbol{p}$ is proportional to the aspect ratio at large aspect ratios (Sect. 2.2). We find the same behaviour in the flow past a sphere: the higher the aspect ratio, the higher is the period of oscillation in $\boldsymbol{p}$. At $R = 20$, it is necessary to run the problem up to $t = 40$ in order to calculate the average drag force accurately.

The results are summarized in Fig. 7, where the reduced viscosity is plotted against the volume fraction at three different aspect ratios. Plotted in the same figure are the falling-sphere data on suspensions of blunt-ended rods and nylon fibres at aspect ratio 19.8. It is clear that this theory agrees reasonably well with the experimental data. However, with the maximum volume fraction $A = 0.27$, the non-linear behaviour sets in at $\Phi \approx 0.075$. With $A = 0.46$, a much better fit to the experimental results can be achieved. The transition from the linear to cubic behaviour can be better seen by plotting the specific viscosity $\eta_{sp} = \eta_r - 1$ vs the volume fraction, as shown in Fig. 8. Subtracting 1 from η_r has the effect of accentuating the linear regime, and, with a limited number of data points between $0.1 < \Phi < 0.2$, one can certainly fit a cubic relation to the $\eta_{sp} - \Phi$ curve. The apparent linear to cubic transition displayed by the numerical results is indeed an artifact of the method of plotting and the limited range of volume fraction considered. The solid lines connecting the numerical points at high volume fractions are not the continuation of the lines of best fit; they are in fact the asymptotic results, which will be discussed next.

3.3 Asymptotic solution

Asymptotic solutions at high-volume fractions ($\Phi/A \to 1$) can be found by rewriting the extra stress as

$$S = \eta f(\Phi, R)\left(\frac{2}{f}\boldsymbol{D} + 2\boldsymbol{D}:\boldsymbol{pppp}\right) .$$

If we now normalize the stresses and the pressure with respect to $\eta f(\Phi, R)$, then the scaled problem corresponds to a Newtonian viscosity of $1/f$. At high volume fractions ($\Phi/A \to 1$), $1/f$ goes to zero and the Newtonian-contributed stress ($2/f\boldsymbol{D}$) is of lower order than the fibre-contributed stress ($2\boldsymbol{D}:\boldsymbol{pppp}$) and can be neglected. Thus, in the scaled problem, only the aspect ratio of the fibres enters the problem (via the evolution equation for $\boldsymbol{p}$) and not the volume fraction. This scaled problem can be solved to supply the scaled drag force acting on the sphere. The dimensional drag force on the sphere is this scaled drag force multiplied by $f(\Phi, R)$. In this manner, we find that the asymptotic formula for the reduced viscosity is given precisely by

$$\eta_r = k\frac{\Phi(2-\Phi/A)}{(1-\Phi/A)^2} ,$$

which is similar to the simple shear case, where $k = 2.42 \pm 0.05$ for $R = 5$, $\theta = 90°$ (initially the fibres are all aligned in the radial direction), $k = 4.7 \pm 0.1$ for $R = 10$, $\theta = 90°$, and $k = 14.5 \pm 0.1$ for $R = 20$, $\theta = 90°$.

The errors on k are obtained from the standard deviations of the time averages over different time intervals of the dimensionless drag forces. Thus, the reduced viscosity at high-volume fraction, as measured by the falling sphere, is considerably higher than that measured in the simple shear flow. At the aspect ratio of 20, the falling-sphere reduced viscosity is about seven times higher than the simple shear-reduced viscosity if $\Phi > 0.10$.

The intrinsic viscosity derived from the asymptotic results above for $R = 20$ is about 29. A linear-regression analysis on the numerical data in the range of $0.01 \leq \Phi \leq 0.075$ yields an intrinsic viscosity of 26, which is surprisingly close to the observed value of 28.5 [1]. In the finite-element simulation [20], an intrinsic viscosity of the order 10 was predicted for the same aspect ratio of 20. The constitutive relation used in [20] differs from ours in two aspects: the functional form for f is different to ours, and a streamline tracking scheme was used in [20]. The functional form for f is not a critical issue here at large aspect ratios and small volume fractions. The streamline scheme, however, changes the character of the flow from being intrinsically unsteady to steady flow. It would be worthwhile to perform a similar unsteady finite-element simulation. We have also implemented the full alignment assumption in the boundary-element code using the present model. For the case of $R = 20$, we find that the value of k reduces from 14.5 to 7.1. This yields an intrinsic viscosity of about 14.2, which is 42% higher than the value found by the finite-element simulation [20]; this is due to the fact that our frictional resistance ($R^2/(\ln 2R - 1.5)$) is about 68% higher than the frictional resistance used in the finite-element study ($R^2/\ln 2R$) at the aspect ratio of 20. By forcing the fibres to align with the streamlines, the full alignment assumption clearly underestimates the drag force on the sphere, which leads to a reduced intrinsic viscosity.

The initial orientation of the fibres also has a noticeable influence at high volume fraction and at short time ($t < 10$), especially at large aspect ratios. Plotted in Fig. 9 is the value of k as a function of time for three different initial orientations of the fibres of aspect ratio 20. It is clear from the figure that an initial random suspension has the highest reduced viscosity if a short time average ($t < 10$) of k is taken. However, the long time averages of k ($10 < t < 40$) for the three initial orientations are not significantly different from each other. When $\theta = 0$ we find the long time average of k is 14.7 ± 0.3; this value is 14.8 ± 0.1 when the initial orientation of the fibres is random. There are some limited experimental data [5], which suggest that the reduced viscosity of an initially ran-

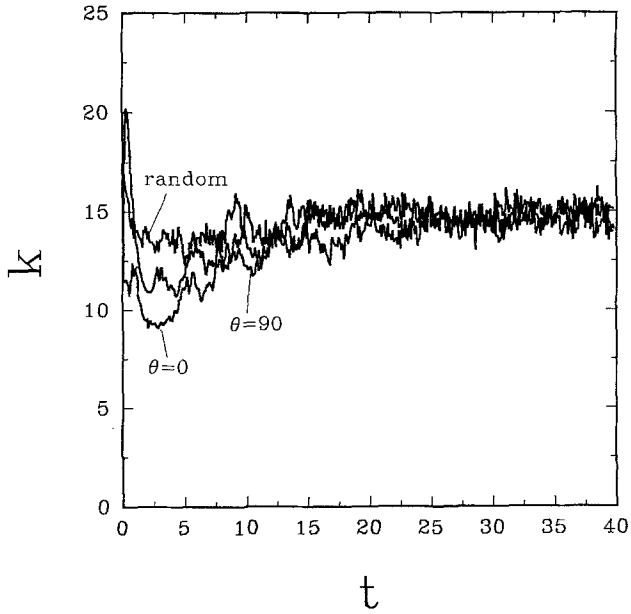

Fig. 9. k as a function of time for different initial orientations of the fibres. At long time, the initial states of the fibres do not have a large effect on k

domized suspension at a volume fraction of 0.05 is about 50% higher than the corresponding value for an initially aligned (with the tube axis) suspension. The trend predicted by the theory is correct, but the theory cannot predict the magnitude of the change in the reduced viscosity. Note that the fibres used in Mor and Graham's experiments [5] are comparable in size to the falling sphere; their inertia may be a significant factor that needs to be considered.

3.4 Kinematics

The kinematics are different from Newtonian kinematics, especially at high volume fraction. Strictly speaking, there are no streamlines in this problem, because the kinematics are intrinsically unsteady. However, the "streamlines" serve as a useful device for comparing the results with the Newtonian solution. We find that the non-Newtonian streamlines are slightly non-symmetric in contrast to the Newtonian streamlines. The asymmetry is seen most clearly when we plot contours of the modified stream function

$$\psi_1 = \psi - \tfrac{1}{2}r^2 \ ,$$

as shown in Fig. 10; ψ_1 is the stream function that corresponds to the moving/falling sphere in a stationary cylinder. The fore-and-aft symmetry is no longer present in the non-Newtonian case. This is reminiscent of the viscoelastic case, where a shift in the streamlines was found [32–37].

Similarly, the contours of the axial and radial velocities are not symmetric about the plane $x = 0$. This symmetry also is not present in the viscoelastic flow [32–37]. At low volume fractions, however, the kinematics are similar to the Newtonian kinematics [21].

The orientation of the microstructure along the tube is shown in Fig. 11 at time $t = 40$ for $R = 20$, $\Phi = 0.10$, but with different initial orientation of the fibres. In this figure, $\boldsymbol{p}$ is represented by an arrow. It is most interesting to find that the evolution of the microstructure can depend dramatically on the initial conditions of $\boldsymbol{p}$. However, at long times the fibres tend to align themselves with the tube axis in the downstream-wake region regardless of their initial configurations. The overall orientations of the fibres at time $t = 40$ are quite similar, despite their different initial states. This explains why the average drag force on the sphere is only weakly dependent on the initial orientation of the fibres over long time. The alignment of the fibres behind the sphere has been observed [5] with semi-concentrated systems. The falling ball, therefore, may be used as a device to partially align fibres. A physical explanation of this phenomenon is that the flow along the centreline in the downstream region of the sphere is extensional in nature, see, for example [28]. Such a flow is capable of aligning the fibres well. Even if the fibres initially are randomly placed, they tend to re-arrange themselves with the flow; the transition from dis-ordered to ordered states takes place in about 4 dimensionless time, especially for the fibres in front of the sphere next to the tube wall.

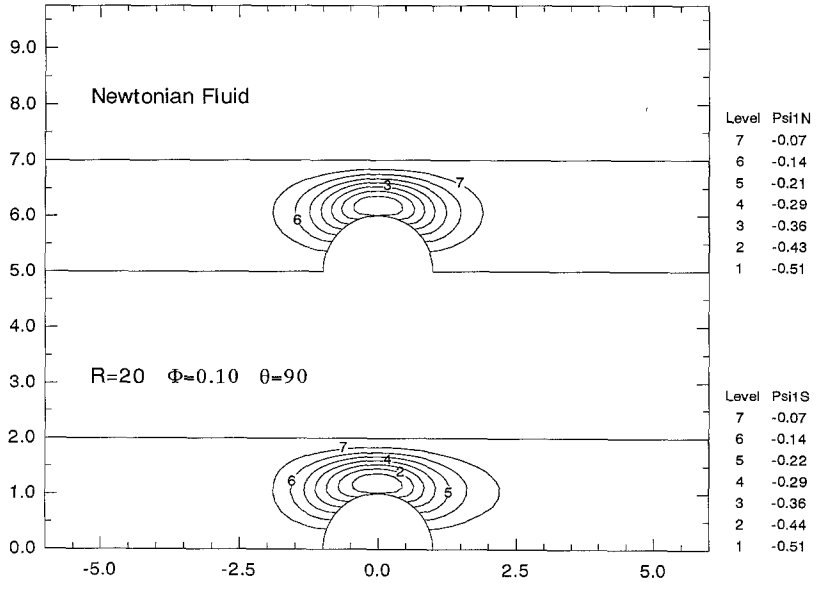

Fig. 10. Contours of $\psi_1 = \psi - \frac{1}{2}r^2$. ψ_1 is the stream function that corresponds to a moving sphere in a stationary cylinder. The asymmetry is evident in the non-Newtonian case

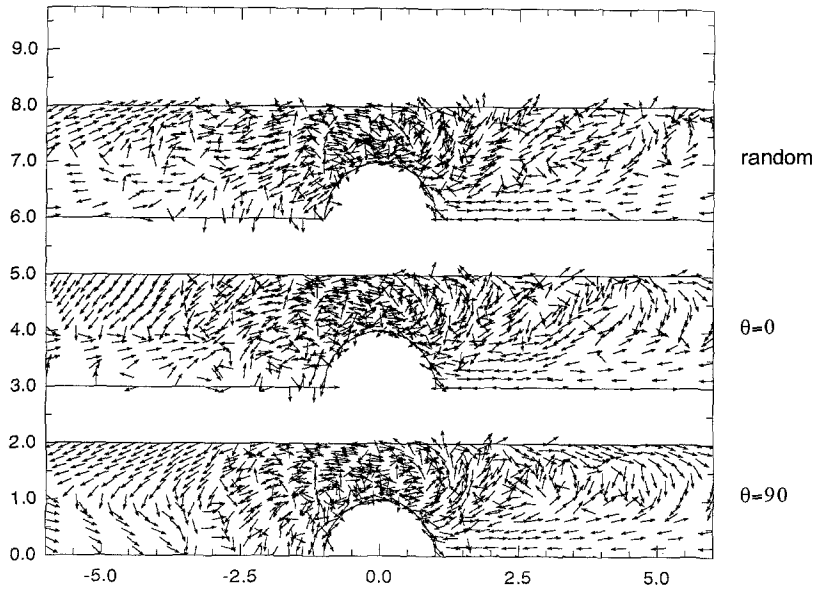

Fig. 11. Orientation of the microstructure at $t = 40$ for $R = 20$ and $\Phi = 0.10$. Note that most of the fibres behind the sphere align with the tube axis. The fibres are also well-ordered in front of the sphere near the tube wall, especially in the case where the fibres' orientation is randomized initially. This may be due to the shear-flow component brought about by the presence of the wall

4. Final remarks

We proposed a new constitutive equation for suspensions of rods of aspect ratios from 5 to 30. The constitutive equation is of the same functional form as the Transversely Isotropic Fluid (TIF) model of Ericksen [14]. A low-volume fractions, the new model reduces properly to the leading terms of the constitutive equation for a dilute suspension of prolate spheroids [18]. There are three parameters in the model: the aspect ratio R, the volume fraction Φ and a parameter A, which plays the role of the maximum volume fraction. The last parameter is estimated to be 0.27, using the shear-flow data from Kitano et al. [22], and the resulting model is used to solve the flow past a sphere placed at the centreline of a cylinder, using a boundary-element method.

Numerical results show that the flow is intrinsically unsteady, and the long time behaviour of the drag force depends only weakly on the initial configuration of the microstructure. The reduced viscosity deduced from the drag force by a time average agree well with the experimental data of Milliken et al. [1]. At high-volume fractions, it is possible to solve a scaled problem to supply the asymptotic formula for the reduced viscosity. The linear-to-cubic transition in the specific viscosity vs the volume fraction plot occurs at a volume fraction of about 0.075 if $A = 0.27$. For this to occur at $\Phi = 0.125$, as observed by Milliken et al. [1], the maximum volume fraction should be about 0.46.

Furthermore, we find that the kinematics are no longer Newtonian-like at high-volume fractions, and there may be thin boundary layers across which the orientation vector $\boldsymbol{p}$ flips its direction. The resolution of these boundary layers makes it difficult to analyze complex flows of suspensions. In the downstream region (i.e., behind the falling sphere) and over long time, the fibres align themselves along the tube axis in agreement with some experimental observation.

An alternative approach is to solve this problem as a many-body problem, for example, by Stokesian dynamic simulation [44]. This latter technique is still in its preliminary stage, and any other numerical schemes for solving many body problems are not viable alternatives for present-day computers. The continuum approach will yield useful results in the preseeable future.

Acknowledgement

This research is funded by an Australian Research Grant Scheme. The support is gratefully acknowledged. Portions of this work were supported by a grant from the Division of Engineering and Geosciences, Office of Basic Energy Science, U.S. Department of Energy (KC04106). Work performed at Los Alamos Laboratory was sponsored by the U.S. Department of Energy under contract W-7405-ENG-36 with the University of California. We wish to thank the staff of the Technical Engineering Support Group at Los Alamos for providing the facilities and support that allowed this study to be performed.

References

1. Milliken WJ, Gottlieb M, Graham AL, Mondy LA, Powell RL (1989) Fluid Mech 202:217
2. Brenner H (1974) Int J Multiphase Flow 1:195
3. Metzner AB (1985) J Rheology 29:739
4. Ganani E, Powell RL (1985) J Composite Materials 19:194
5. Morr R, Graham AL (unpublished data)
6. Graham AL, Mondy LA, Altobelli SA (1990) private communication
7. Goettler LA, Lambright AJ, Leib RI, DiMauro PJ (1981) Rubber Chem Technol 54:277
8. Givler RC, Crochet MJ, Pipes RB (1983) J Composite Materials 17:330
9. Jeffery GB (1922) Proc Roy Soc Lond A102:161
10. Lipscomb II GG, Denn MM, Hur DU, Boger DV (1988) J Non-Newt Fluid Mech 26:297
11. Mewis J, Metzner AB (1974) J Fluid Mech 62:593
12. Weinberger CB, Goddard JD (1974) Int J Multiphase Flow 1:465
13. Kizior TE, Seyer FA (1974) Trans Soc Rheol 18:271
14. Ericksen JL (1960) Arch Rat Mech Anal 3:117
15. Giesekus H (1962) Rheol Acta 2:50
16. Hand GL (1961) Arch Rat Mech Anal 7:81
17. Cox RG, Brenner H (1971) Chem Eng Sci 26:65
18. Leal LG, Hinch EJ (1971) J Fluid Mech 46:685
19. Leal LG, Hinch EJ (1973) Rheol Acta 12:127
20. Rosenberg J, Denn MM, Keunings R (1990) J Non-Newt Fluid Mech (in press)
21. Phan-Thien N, Zheng R, Graham AL (1990) J Stat Phys (in press)
22. Phan-Thien N, Tran-Cong T, Graham AL (1990) J Fluid Mech (submitted)
23. Kitano T, Kataoka T, Shirota T (1981) Rheol Acta 20:207
24. Evans J (1975) PhD Thesis. University of Cambridge, Cambridge
25. Dinh SH, Armstrong RC (1984) J Rheol 28:207
26. Fifth Workshop on Numerical Methods in Non-Newtonian Flows (1988) J Non-Newt Fluid Mech 29:ix
27. Brown R, Armstrong RC (1989) Paper presented at the 6th Workshop on Numerical Methods in Non-Newtonian Flows, Denmark
28. Zheng R, Phan-Thien N, Tanner RI (1990) 6th Workshop on Numerical Methods in Non-Newtonian Flows. J Non-Newt Fluid Mech, in press
29. Acharya A, Mashelkar RA, Ulbrecht J (1976) Rheol Acta 15:454
30. Bird RB, Hassager O, Armstrong R (1988) Dynamics of polymeric liquids: Fluid Mechanics, vol 1, 2nd edn. Wiley, New York
31. Adachi K, Yoshioka N, Sakai K (1977/78) J Non-Newt Fluid Mech 3:107
32. Tiefenbruck G, Leal LG (1982) J Non-Newt Fluid Mech 10:115
33. Gu Dazhi, Tanner RI (1985) J Non-Newt Fluid Mech 17:1
34. Hassager O, Bisgaard C (1983) J Non-Newt Fluid Mech 12:153
35. Luo XL, Tanner RI (1986) J Non-Newt Fluid Mech 21:179
36. Crochet MJ (1988) Paper presented at the 10th Int Congr Rheology, Sydney, p 19
37. Sugeng F, Tanner RI (1986) J Non-Newt Fluid Mech 20:281
38. Acrivos A, Jeffrey DJ, Gadala-Maria F, Herbolzheimer E (1979) Final Report, AF-1085, Research Project 314-1, Chap 3. Stanford University, Stanford
39. Ivanov Y, Van de Ven TGM, Mason SG (1982) J Rheol 26:213
40. Batchelor GK (1970) J Fluid Mech 41:545
41. Ganani E, Powell RL (1986) J Rheology 30:995
42. Phan-Thien N, Sugeng F, Tanner RI (1987) J Non-Newt Fluid Mech 24:97
43. Happel J, Brenner H (1973) Low Reynolds number hydrodynamics. Noordhoff, Leiden
44. Brady JF, Bossis G (1988) Ann Rev Fluid Mech 20:111

(Received June 1, 1990;
in revised form September 14, 1990)

Correspondence to:

Prof. Nhan Phan-Thien
Department of Mechanical Engineering
University of Sydney
Sydney, NSW 2006, Australia